Unmanned Systems, Vol. 14, No. 2 (2026) 441–459

DOI: 10.1142/S230138502650010X

UNMANNED SYSTEMS
https://www.worldscientific.com/worldscinet/us

Design and Experimental Attitude Control of Quadrotor Via Optimized Adaptive IT-2 FLC Integrated with Nonlinear FOPID

Qiyuan Wang[*,¶,**], Caiping Zhao[†], Yanchun Liu[‡,‖,**], Hongxue Qu[‡], Xuejun Feng[§]

[*]*School of Computer Science, Beijing Information Science and Technology University, Beijing 100101, P. R. China*

[†]*C-EPRI Electric Power Engineering Co. Ltd., Nari Group Corporation, Beijing 100192, P. R. China*

[‡]*Department of Computer and Software Engineering, Shandong College of Electronic Technology, Jinan 250200, Shandong, P. R. China*

[§]*Inspur Communication Information Systems Co., Ltd., Jinan 250101, Shandong, P. R. China*

This paper presents an adaptive Interval Type-2 Fuzzy Logic Controller (IT2-FLC) integrated with a nonlinear Fractional-Order Proportional Integral-Derivative (FOPID) controller for quadrotor attitude control. The adaptive mechanism, based on sliding surfaces, tunes the controller parameters in real-time. Moreover, the fuzzy system is integrated with a nonlinear FOPID controller. Unlike the fixed gains of the conventional FOPID, the nonlinear variant dynamically adjusts its parameters in real-time. The Grey Wolf Optimizer (GWO) is used to optimize both controller and fuzzy system parameters, minimizing the Integral of the Absolute Error (IAE). To validate the effectiveness of the proposed controller, three configurations — IT2-FLC integrated with FOPID, adaptive IT2-FLC integrated with FOPID and IT2-FLC integrated with nonlinear FOPID — are designed for the attitude control of a quadrotor, all aiming to achieve the same objective function. The results show that nonlinear gain alone improves performance more than the adaptive structure alone in all axes. For the roll axis, nonlinear gain reduces IAE and RMSE by 55.08% and 40.80%, respectively, while the adaptive structure achieves smaller improvements of 34.62% and 17.24%. In the pitch axis, nonlinear gain reduces IAE and RMSE by 37.36% and 18.10%, compared to 30.27% and 8.45% with the adaptive structure. Combining nonlinear gain with the adaptive structure leads to the best performance in all cases, with the largest improvements in IAE, MAE and RMSE observed in the roll and yaw axes.

Keywords: Attitude control; adaptive control; fractional calculus; nonlinear gain; type-2 fuzzy logic; GWO.

1. Introduction

The control of quadrotors is vital due to their broad applications. The ability to have precise control allows quadrotors to accomplish complex tasks with accuracy and efficiency. These tasks include conducting aerial surveillance, delivering packages and carrying out search and rescue operations. However, controlling quadrotors presents unique challenges. These challenges encompass the inherent nonlinear dynamics of the quadrotor system, constrained payload capacity, environmental uncertainties and the imperative for real-time decision-making. Additionally, quadrotors are susceptible to external disturbances, which can affect their stability and performance. Designing effective control algorithms to address these

Received 21 September 2024; Accepted 19 January 2025; Published 20 June 2025. This paper was recommended for publication in its revised form by editorial board member, Wen-Hua Chen.
Email Addresses: [¶]*wangqiyuan0418@126.com*, [‖]*1720372362@163.com*
[**]Corresponding authors.

challenges is essential for ensuring the safe and reliable operation of quadrotors, while also achieving the desired flight characteristics, maneuverability and responsiveness.

In Unmanned Aerial Vehicle (UAV) applications, various factors introduce inherent uncertainties. These uncertainties include inadequate modeling, aerodynamic disturbances, environmental variations, rotor damage, battery drain, ground effects, as well as sensor and actuator noise [1–4]. To address these uncertainties, researchers have developed several anti-disturbance controllers, such as the nonlinear Model Predictive Control (MPC) technique [5, 6] and the Sliding Mode Control (SMC) method [7, 8]. The MPC approach relies on a precise system model, while the SMC method is limited by the occurrence of unexpected chattering phenomena, which restricts its applicability in many industrial systems. In light of these challenges, Fuzzy Logic Control (FLC) has emerged as an alternative solution to enhance the robustness of control systems in the presence of uncertainties and external disturbances [9, 10]. Among the various types of FLCs, Type-1 FLCs (T1-FLCs) are well-known and widely employed [11, 12]. Interval Type-2 FLCs (IT2-FLCs) offer enhanced robustness and better handling of uncertainties compared to T1-FLCs due to their ability to model and manage higher degrees of uncertainty within the system [13]. Hence, researchers have recently paid significant attention to IT2-FLCs [14–16].

IT2-FLCs have demonstrated their capability in handling rule uncertainties, positioning them as suitable solutions for addressing the challenges associated with controlling quadrotors. Hailemichael and Karimoddini [17] developed a robust IT-2 Takagi–Sugeno–Kang (TSK) FLC specifically designed for the attitude control of UAVs, showcasing its effectiveness in capturing and accommodating uncertainties. Al-Mahturi *et al.* [18] presented an enhanced self-adaptive IT2-FLC system tailored for quadcopter drone stabilization. Le *et al.* [19] proposed a multilayer IT2-FLC for quadcopter UAVs, offering the capacity to approximate complex nonlinear relationships within the system. Dombi and Hussain [20] employed IT2 fuzzy sets in the antecedent part and intervals in the zero-order TSK fuzzy system's consequent part, resulting in improved accuracy and interpretability of the system. Shirzadeh *et al.* [21] proposed a robust control strategy that is adaptive and based on a type-2 fuzzy neural network. This control strategy has been specifically developed to accurately track desired trajectories of quadrotors.

On the other hand, the integration of fuzzy logic with conventional control systems, known as hybrid control systems, presents a promising approach for enhancing system performance. By combining the precision and stability of classical control techniques with the adaptability and intuitive reasoning capabilities inherent in fuzzy logic, these hybrid systems enable robust control in complex and uncertain environments. Recent studies have notably demonstrated the efficacy of employing fuzzy systems for fine-tuning control method parameters. Various instances include fuzzy PID [22], adaptive fuzzy PID [23], self-adaptive neuro-fuzzy PID [24], adaptive fuzzy sliding mode [25] and adaptive fuzzy backstepping control [26].

Fractional-Order Proportional Integral-Derivative (FOPID) controllers, an advancement of traditional PID controllers, provide a superior control framework, which allows for a more flexible and nuanced response to dynamic system changes, essentially offering an expanded tuning spectrum, thereby improving the stability and performance of control systems across a wider range of operating conditions [27]. Several studies have demonstrated the effectiveness of integrating FO concepts with control methods to address the challenges encountered in quadrotor dynamics. Labbadi *et al.* [28] proposed a continuous FO improved super twisting PID sliding-mode control technique. This approach effectively tackles issues such as parameter uncertainties, nonlinearities and aerodynamic disturbances. Guettal *et al.* [29] combined the advantages of FO calculus, backstepping control and neural networks to handle the uncertainties and nonlinearities in quadrotor dynamics. Their approach showcased improved control performance in challenging operating conditions. Ansarian and Mahmoodabadi [30] introduced a fuzzy adaptive robust FO approach, which demonstrated enhanced performance in managing the nonlinear dynamics of unmanned flying systems. These studies highlight the potential of using FO techniques to enhance control strategies and address the complexities associated with quadrotor dynamics.

Additionally, precise optimization of controller parameters is crucial for attaining the desired performance of control systems, particularly in quadrotor control design, where minimizing control effort and output errors are key objectives. Striking a balance between these criteria is vital. Meta-heuristic algorithms, such as the genetic algorithm [31], particle swarm optimization [32], Bat algorithm [33], grey wolf optimization [34], cuckoo search [35], bee algorithm [36] and ant colony optimization [37], have received significant attention as effective methodologies for navigating and resolving the intricate trade-offs involved in achieving a harmonious balance among these criteria.

While much of the existing literature has focused on the individual effects of nonlinear gain and adaptive structures within IT2-FLC controllers, often incorporating sliding surfaces, there remains a notable gap in the integration of these approaches. A comprehensive review of recent research reveals this unexplored area, emphasizing the need for a more holistic control strategy that synergistically combines the advantages of both adaptive fuzzy logic and nonlinear gain compensators. To address this gap, the proposed hybrid controller introduces a novel cascade configuration that integrates IT2 fuzzy systems, sliding surfaces and nonlinear FOPID compensators. This integration facilitates more robust and adaptive control for nonlinear UAV systems. In this hybrid structure, the scaling coefficients of the fuzzy system are dynamically adapted through an innovative adaptive mechanism based on sliding surfaces. This mechanism enables the real-time adjustment of fuzzy system gains, ensuring that the controller remains responsive to changing conditions and uncertainties during flight. Moreover, the inclusion of a nonlinear FOPID controller further enhances system performance by compensating for the inherent nonlinearities of the UAV. The nonlinear FOPID controller achieves precise control over the UAV's dynamics by dynamically adjusting its gains based on real-time performance feedback. This combined approach not only improves the stability and responsiveness of the UAV system but also provides a comprehensive solution to the challenges of adaptive and nonlinear control in complex, uncertain environments. To demonstrate the effectiveness of the proposed controller, three designs are implemented: IT2-FLC with FOPID, adaptive IT2-FLC with FOPID (a novel contribution), and IT2-FLC with nonlinear FOPID (another novel contribution), all applied to quadrotor attitude control with the same objective function.

2. Quadrotor UAV Dynamic Model

To analyze the motion of a rigid body in three-dimensional space, two separate coordinate frames are established. The first coordinate frame, denoted as $\{B\}$, is specifically designed for the quadrotor and is identified as the aircraft-fixed coordinate system. The $\{B\}$ frame's origin is situated at the center of gravity position, aligning with the principal plane of symmetry. Alongside, a global-fixed reference frame denoted as $\{E\}$ is established to function as the inertial frame. In the $\{E\}$-frame, the position vector of the quadrotor's center of mass is denoted as ${}^{\{E\}}\boldsymbol{\chi} = [x\ y\ z]^T$, and its orientation is represented by the Euler angles vector $\boldsymbol{\Theta} = [\phi\ \theta\ \psi]^T$, $-\pi/2 \leq \phi \leq \pi/2, -\pi/2 \leq \theta \leq \pi/2, -\pi \leq \psi \leq \pi$. These angles correspond to roll (ϕ), pitch (θ) and yaw (ψ), respectively. The $\{B\}$-frame, which is fixed to the vehicle, captures the quadrotor's translational and rotational dynamics. The translational velocity in the body frame is expressed as ${}^{\{\mathbf{B}\}}\mathbf{V} = [u\ v\ w]^T$. Similarly, the angular velocity vector in the body frame is given by ${}^{\{\mathbf{B}\}}\boldsymbol{\omega} = [p\ q\ q]^T$, where p, q, and r are the rates of rotation about the body frame axes (Fig. 1).

The rotational kinematics, which describe the relationship between the angular velocities in the $\{B\}$-frame and the Euler angles, are essential for the control and stability of the quadrotor. Thus, the rotational kinematics governing the relationship between these angular velocities and the Euler angles is expressed as [30]

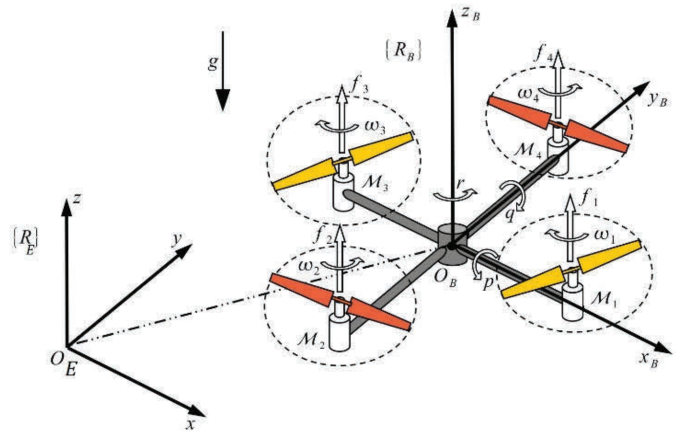

Fig. 1. The schematic representation of quadrotor.

$$\dot{\boldsymbol{\Theta}} = \Phi(\boldsymbol{\Theta})^{\{\mathbf{B}\}}\boldsymbol{\omega} = \begin{bmatrix} \dot{\phi} \\ \dot{\theta} \\ \dot{\psi} \end{bmatrix}$$

$$= \begin{bmatrix} 1 & \sin\phi\tan\theta & \cos\phi\tan\theta \\ 0 & \cos\phi & -\sin\phi \\ 0 & \sin\phi\sec\theta & \cos\phi\sec\theta \end{bmatrix} \begin{bmatrix} p \\ q \\ r \end{bmatrix}, \tag{1}$$

The transformation from the body frame to the Earth frame is described by the rotation matrix $({}^{\{E\}}\mathcal{R}_{\{B\}})$. This matrix is defined according to a 3–2–1 rotation sequence, as follows [30]:

$${}^{\{E\}}\mathcal{R}_{\{B\}}.$$

$$= \begin{bmatrix} \cos\theta\cos\psi & \sin\phi\sin\theta\cos\psi - \cos\phi\sin\psi & \cos\phi\sin\theta\cos\psi + \sin\phi\sin\psi \\ \cos\theta\sin\psi & \sin\phi\sin\theta\sin\psi + \cos\phi\sin\psi & \cos\phi\sin\theta\sin\psi - \sin\phi\cos\psi \\ -\sin\theta & \sin\phi\cos\theta & \cos\phi\cos\theta \end{bmatrix}. \tag{2}$$

The translational dynamics of the quadrotor are analyzed within the inertial frame $\{E\}$, while its rotational dynamics are evaluated within the body frame $\{B\}$. The quadrotor's motion is governed by several critical factors, including the thrust force (F_i) and the aerodynamic moment (Q_i) produced by the four rotors. The resultant combination of thrust forces and aerodynamic moments acting on the quadrotor gives rise to four generalized forces in the body frame $\{B\}$, as delineated in the following equations [12]:

$$U_1 = \sum_{i=1}^{4} F_i = C_T(\omega_1^2 + \omega_2^2 + \omega_3^2 + \omega_4^2), \tag{3}$$

$$U_2 = F_4L - F_2L = Lb(\omega_4^2 - \omega_2^2), \tag{4}$$

$$U_3 = F_3L - F_1L = Lb(\omega_3^2 - \omega_1^2), \tag{5}$$

$$U_4 = \sum_{i=1}^{4} (-1)^{i+1} Q_i = C(\omega_1^2 - \omega_2^2 + \omega_3^2 - \omega_4^2),$$
$$C = \frac{C_M}{C_T}. \tag{6}$$

The variables $\omega_1, \omega_2, \omega_3$ and ω_4 denote the angular velocities of the rotors. Here, C_T represents the thrust coefficient, C_M denotes the moment coefficient, and L signifies the length of each quadrotor's arm. The control inputs for the quadcopter are U_i for $i = 1, 2, 3, 4$, where U_1 represents the total thrust on the quadrotor body along the z_B axis, U_2 and U_3 correspond to roll and pitch inputs, respectively, and U_4 represents the yawing moment. The dynamics of the quadrotor model are derived from the six-degree-of-freedom equations, which are formulated based on the Newton-Euler equations. These equations account for the external forces and moments applied to the quadrotor's center of mass [28].

$$\Sigma \mathbf{F}_{\text{ext}} = m^{\{\mathbf{B}\}}\dot{\mathbf{V}} + {}^{\{\mathbf{B}\}}\boldsymbol{\omega} \times m^{\{\mathbf{B}\}}\mathbf{V}, \tag{7}$$

$$\Sigma \mathbf{M}_{\text{ext}} = I(\dot{{}^{\{\mathbf{B}\}}\boldsymbol{\omega}}) + {}^{\{\mathbf{B}\}}\boldsymbol{\omega} \times I^{\{\mathbf{B}\}}\boldsymbol{\omega}, \tag{8}$$

where m denotes the mass of the quadcopter and $I = \text{diag}(I_x, I_y, I_z)$ represents its inertia matrix. The external forces and moments are described within the body-fixed frame as follows [28]:

$$\Sigma \mathbf{F}_{\text{ext}} = \mathbf{F}_{\text{prop}} - \mathbf{F}_{\text{aero}} - \mathbf{F}_{\text{grav}} - \mathbf{F}_{\text{dis}}, \tag{9}$$

$$\Sigma \mathbf{M}_{\text{ext}} = \mathbf{M}_{\text{prop}} - \mathbf{M}_{\text{aero}} - \mathbf{M}_{\text{gyro}} - \mathbf{M}_{\text{dis}}, \tag{10}$$

where the active forces $\mathbf{F}_{\text{prop}}$ and moments $\mathbf{M}_{\text{prop}}$ generated by the rotors are defined as $\mathbf{F}_{\text{prop}} = [0\ 0\ \sum_{i=1}^{4} F_i]^T \epsilon \mathbb{R}^3$ and $\mathbf{M}_{\text{prop}} = [(F_4 - F_2)L\ (F_3 - F_1)L\ C\sum_{i=1}^{4} (-1)^{i+1} F_i]^T \epsilon \mathbb{R}^3$. The term $\mathbf{F}_{\text{grav}} = m({}^{\{E\}}\mathcal{R}_{\{B\}})^T \mathbf{G}$ is the gravity force with $\mathbf{G} = [0\ 0\ 9.81]^T$. The terms $\mathbf{F}_{\text{aero}} = K_t{}^{\{\mathbf{B}\}}\mathbf{V}$ and $\mathbf{M}_{\text{aero}} = K_r{}^{\{\mathbf{B}\}}\boldsymbol{\omega}$ represent the aerodynamic drag forces and moments, respectively, where K_t and K_r are the diagonal aerodynamic dynamic coefficient matrices. $\mathbf{M}_{\text{gyro}} = \sum_{i=1}^{4} J_R({}^{\{\mathbf{B}\}}\boldsymbol{\omega} \times \mathbf{e}_{\mathbf{z_B}})(-1)^{i+1}\omega_i$, where J_R is the rotor inertia. $\mathbf{F}_{\text{dis}}, \mathbf{M}_{\text{dis}} \epsilon \mathbb{R}^3$ signify parameter uncertainties and external disturbance forces and moments in $\{B\}$, such as wind drags, load variation, ground effects, uneven mass distributions and rotor fluctuations. Utilizing Eqs. (7)–(10), the quadrotor's dynamics can be expressed in the reference frame $\{I\}$ as follows:

$$\ddot{\chi} = \frac{1}{m}{}^{\{I\}}\mathcal{R}_{\{B\}}(\mathbf{F}_{\text{prop}} - \mathbf{F}_{\text{aero}}) - \mathbf{G} - \frac{1}{m}({}^{\{I\}}\mathcal{R}_{\{B\}})^T \mathbf{F}_{\text{dis}}, \tag{11}$$

$$\ddot{\boldsymbol{\Theta}} = (I\Phi(\boldsymbol{\Theta}))^{-1}\Bigg(\mathbf{M}_{\text{prop}} - \mathbf{M}_{\text{aero}} - \mathbf{M}_{\text{gyro}} - \Phi(\boldsymbol{\Theta})\dot{\boldsymbol{\Theta}} \times I\Phi(\boldsymbol{\Theta})\dot{\Theta} - I\left[\frac{\partial\Phi(\boldsymbol{\Theta})}{\partial\theta}\dot{\theta} + \frac{\partial\Phi(\boldsymbol{\Theta})}{\partial\phi}\dot{\phi}\right]\dot{\boldsymbol{\Theta}}\Bigg). \tag{12}$$

To facilitate the control design, the state space representation of the quadrotor UAV is obtained utilizing the preceding analysis. The primary objective of a UAV controller is to achieve the asymptotic convergence of the dynamic state variables $[x(t), y(t), z(t), \psi(t)]$ toward the predetermined trajectories $[x_d(t), y_d(t), z_d(t), \psi_d(t)]$. This objective may be accomplished through employing a combination of block control and sliding mode methodologies. The mathematical expressions (11) and (12) derived are utilized to articulate the system dynamics in the state space formalism [28].

$$\dot{X} = \mathcal{F}(X, U) = f(X) + g(X)U + D \tag{13}$$

with the following state vector X and input vector U:

$$X = (x_1, x_2, \ldots, x_{12})^T \in \mathbb{R}^{12} \quad \text{and } U = (U_1, U_2, U_3, U_4)^T,$$
$$x_1 = \phi, x_2 = \dot{\phi}, x_3 = \theta, x_4 = \dot{\theta}, x_5 = \psi, x_6 = \dot{\psi},$$
$$x_7 = x, x_8 = \dot{x}, x_9 = y, x_{10} = \dot{y}, x_{11} = z, x_{12} = \dot{z}. \tag{14}$$

Therefore

$$\mathcal{F}(X,U) = \begin{bmatrix} x_2 \\ \left(\dfrac{I_y - I_z}{I_x}\right)x_4x_6 - \dfrac{J_R}{I_x}x_4\omega_r + \dfrac{L}{I_x}U_2 + \dfrac{D_\phi}{I_{xx}} + A_{\dot{\phi}} \\ x_4 \\ \left(\dfrac{I_z - I_x}{I_y}\right)x_2x_6 + \dfrac{J_R}{I_y}x_2\omega_r + \dfrac{L}{I_y}U_3 + A_{\dot{\theta}} + \dfrac{D_\theta}{I_{yy}} + A_{\dot{\theta}} \\ x_6 \\ \left(\dfrac{I_x - I_y}{I_z}\right)x_4x_2 + \dfrac{1}{I_z}U_4 + \dfrac{D_\psi}{I_{zz}} + A_{\dot{\psi}} \\ x_8 \\ \dfrac{U_1}{m}(\cos x_1 \sin x_3 \cos x_5 + \sin x_1 \sin x_5) + \dfrac{D_x}{m} + A_x \\ x_{10} \\ \dfrac{U_1}{m}(\cos x_1 \sin x_3 \sin x_5 - \sin x_1 \cos x_5) + \dfrac{D_y}{m} + A_y \\ x_{12} \\ -g + \dfrac{\cos x_1 \cos x_3}{m}U_1 + \dfrac{D_z}{m} + \mathrm{A}_z \end{bmatrix}$$

$$= \begin{bmatrix} x_2 \\ \left(\frac{I_y - I_z}{I_x}\right) x_4 x_6 - \frac{J_R}{I_x} x_4 \omega_r \\ x_4 \\ \left(\frac{I_z - I_x}{I_y}\right) x_2 x_6 + \frac{J_R}{I_y} x_2 \omega_r \\ x_6 \\ \left(\frac{I_x - I_y}{I_z}\right) x_4 x_2 \\ x_8 \\ 0 \\ x_{10} \\ 0 \\ x_{12} \\ -g \end{bmatrix} + \begin{bmatrix} 0 \\ \frac{L}{I_x} U_2 \\ 0 \\ \frac{L}{I_y} U_3 \\ 0 \\ \frac{1}{I_z} U_4 \\ 0 \\ \frac{U_1}{m}(\cos x_1 \sin x_3 \cos x_5 + \sin x_1 \sin x_5) \\ 0 \\ \frac{U_1}{m}(\cos x_1 \sin x_3 \sin x_5 - \sin x_1 \cos x_5) \\ x_{12} \\ \frac{\cos x_1 \cos x_3}{m} U_1 \end{bmatrix} + \begin{bmatrix} 0 \\ \frac{D_\phi}{I_{xx}} + A_{\dot{\phi}} \\ 0 \\ \frac{D_\theta}{I_{yy}} + A_{\dot{\theta}} \\ 0 \\ \frac{D_\psi}{I_{zz}} + A_{\dot{\psi}} \\ 0 \\ \frac{D_x}{m} + A_x \\ 0 \\ \frac{D_y}{m} + A_y \\ 0 \\ \frac{D_z}{m} + A_z \end{bmatrix}$$

$$= f(X) + g(X)U + D \tag{15}$$

while ω_r denotes the overall speed of the rotors. The value of ω_r can be determined as follows:

$$\omega_r = -\omega_1 + \omega_2 - \omega_3 + \omega_4 \tag{16}$$

and

$$\mathbf{A}_F = \frac{1}{m} {}^{\{I\}}\mathcal{R}_{\{B\}} \mathbf{F}_{\text{aero}} = [A_x, A_y, A_z]^T, \mathbf{A}_T = I^{-1}\mathbf{M}_{\text{aero}} = [A_{\dot{\psi}}, A_{\dot{\theta}}, A_{\dot{\phi}}]^T. \tag{17}$$

The terms D_x, D_y and D_z represent the external disturbance forces acting along the x_I, y_I and z_I axes, respectively. The symbols D_ϕ, D_θ and D_ψ specifically denote external disturbance torques acting within the system. $\mathbf{A}_F$ and $\mathbf{A}_T$ represent the resultant aerodynamic forces and moments, respectively, as defined in the inertia reference frame I. It is worthwhile to note that the translations depend on the angles.

The term $\mathbf{\Lambda} = \Delta f(\mathbf{X}) + \Delta g(\mathbf{X})\mathbf{U} + \mathbf{D}$ is regarded as a lumped disturbance, encompassing both parameter uncertainties and external disturbances. Here, Δf and Δg denote the parameter uncertainties arising from variations in the system parameters such as mass and moment of inertia.

3. Control Architecture

The general schematic for controlling a quadrotor is presented in Fig. 2. The proposed controller system, as illustrated in Fig. 3(d), introduces an enhanced feature by integrating IT2 fuzzy sets into its structure. The inclusion of these fuzzy sets is crucial for accurately representing and communicating uncertainties in membership grades by utilizing the concept of the Footprint of Uncertainty (FOU). By implementing FOU, the controller system gains a higher level of flexibility in handling and controlling the inherent uncertainties within the system. In addition, finding proper values for the gains is important for controller design. Sliding mode concepts are used to formulate the time-dependent relations for them. The determination of the influence of input variables in a fuzzy system is of utmost importance and can be achieved through adaptively modifying the input scaling factors using the sliding mode concept. In this approach, the sliding surface is computed based on the error between the state variables, which serves as the input for the fuzzy logic controller. The ability to dynamically modify scaling factors empowers the controller to demonstrate enhanced flexibility and agility, thereby amplifying its effectiveness in handling a wide range of input scenarios. The integration of adaptive gains empowers the controller to effectively address the nonlinear dependencies

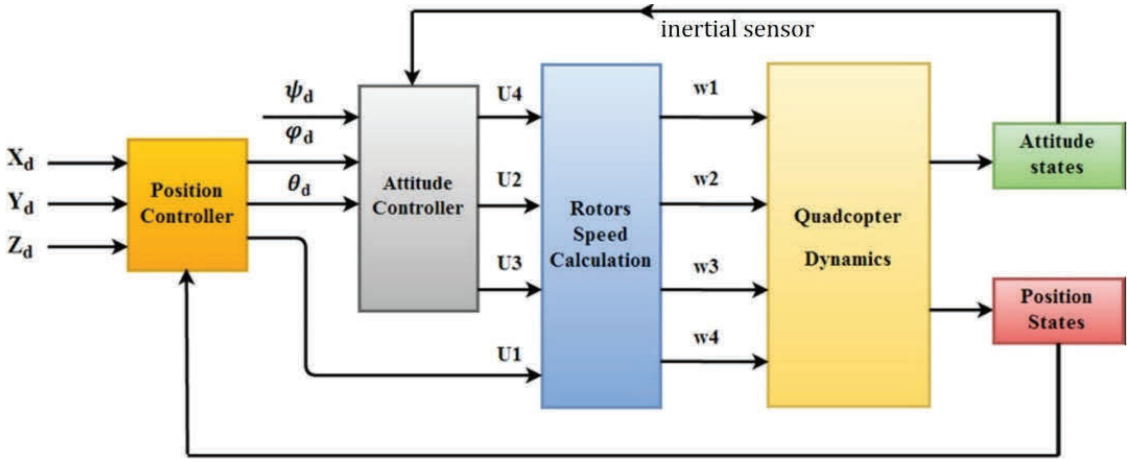

Fig. 2. General schematic of the quadrotor control system.

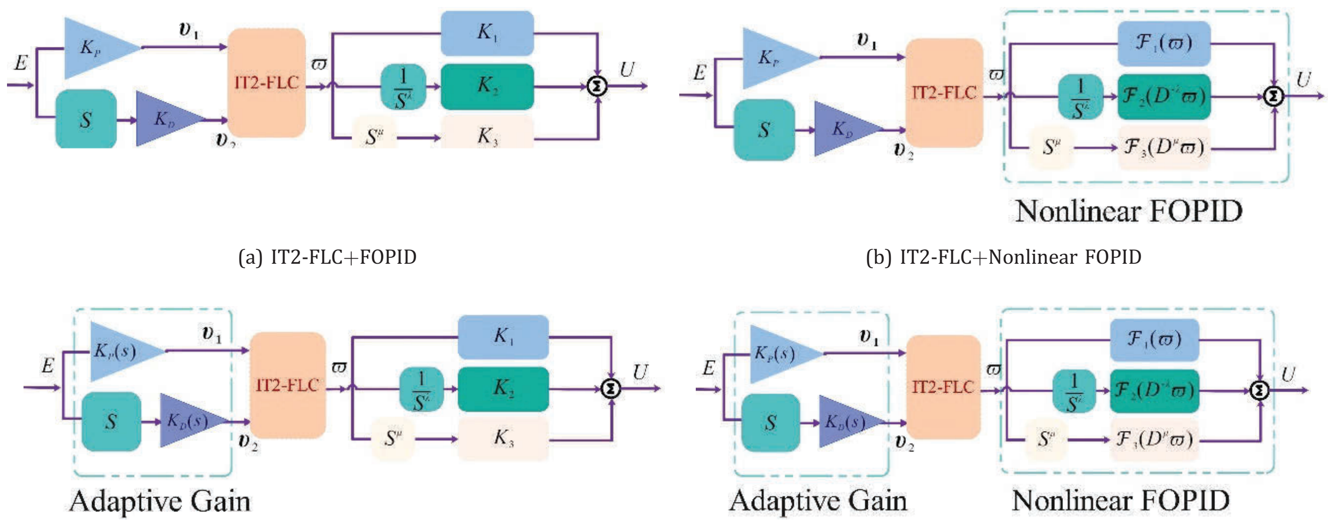

(a) IT2-FLC+FOPID

(b) IT2-FLC+Nonlinear FOPID

(c) Adaptive IT2-FLC+FOPID

(d) Adaptive IT2-FLC+Nonlinear FOPID

Fig. 3. Structure of the proposed hybrid controller used for a quadrotor.

between input parameters and target outputs, thereby leading to enhanced system performance. Additionally, a nonlinear FOPID controller is integrated into the IT-2 FLC. This integration leads to enhanced control performance and improved system stability. The nonlinear FOPID controller surpasses the classical FOPID by dynamically adapting its parameters in real-time. Notably, the nonlinear FOPID controller exhibits the advantage of dynamically adjusting its parameters in response to changing operating conditions. In contrast, the classical FOPID controller relies on fixed proportional, integral and derivative gains, which may yield suboptimal performance when confronted with nonlinearities. Conversely, the nonlinear FOPID controller can adapt its gains in real-time, thereby enhancing its responsiveness and robustness across a broader range of system dynamics. By incorporating adaptive elements, it effectively tracks and controls nonlinear processes, providing a more accurate and stable response compared to traditional FOPID controllers. The proposed hybrid control strategy combines the strengths of adaptive gains, fractional order calculus and fuzzy logic-based decision-making, offering a robust and adaptive approach to address the complexities and nonlinearity of dynamic systems. To further analyze the impact of adaptive gain and nonlinear gain on system performance and investigate their respective effects, three additional controllers are introduced in Fig. 3.

The initial part of the controller introduces an adaptive type-2 fuzzy controller, featuring the adjustment of the input gain of the fuzzy system through the introduction of a sliding surface incorporated with nonlinear FOPID.

Consequently, several definitions of fractional-order operators are delineated.

Definition 1. The Caputo FO derivative employed in the controller design is provided by [38]:

$$ {}_0^C D_t^{\mu} U(t) = \frac{1}{\Gamma(a-\mu)} \int_0^t (t-\tau)^{a-\mu-1} U^{(a)}(\tau) d\tau. \quad (18) $$

Here, μ signifies the derivative order, while the symbol a denotes either the integer supremum or the least upper bound of μ, under the constraint that $a-1<\mu<a$. Moreover, $U(t)$ represents a continuously time-variant function, with the Gamma function denoted as $\Gamma(.)$.

Definition 2. FO integration, denoted as $D_{0,t}^{-\lambda}(U)$, is defined as follows:

$$ D_{0,t}^{-\lambda} U(t) = \frac{1}{\Gamma(\lambda)} \int_0^t (t-\tau)^{\lambda-1} U(\tau) d\tau, \quad (19) $$

where μ and λ correspond to the FO integrator and FO differentiators, respectively.

Additionally, it has been proposed that using adaptive approaches is a very effective way to determine out the scaling gains (K_P and K_D) of the inputs as the FLC uses. This methodology entails the incorporation of sliding mode concepts to establish the relationships governing these control gains. As a result, the determination of the sliding surfaces is facilitated through the error of the state variables in the subsequent way:

$$ S_i = \dot{e}_i + \lambda_i e_i, \quad i = \phi,\ \theta \quad \text{and} \quad \psi, \quad (20) $$

where λ_i is a positive parameter and e_i is the considered state's error. Using the gradient descent method, the proportional and derivative gains of the suggested controller (K_P and K_D) can be calculated as adaptive time-dependent coefficients in the way shown as follows [30–39]. The proof of the adaptive gain is provided in [39].

$$ \dot{K}_{Pi} = -\gamma_{Pi} S_i e_i, \quad (21) $$

$$ \dot{K}_{Di} = -\gamma_{Di} S_i \frac{de_i}{dt}, \quad (22) $$

where γ_{Pi} and γ_{Di} are positive coefficients.

The fuzzy systems suggested to adjust positive parameters λ_i (ϕ, θ and ψ) of the sliding surfaces introduced in Eq. (20), employ the singleton fuzzifier, product inference engine and center average defuzzifier [30].

Moreover, the nonlinear gain, represented as $K(\varpi)$, is a function of $\varpi(t)$ within the control system framework. This nonlinear gain is essentially a mathematical function that operates on the signal term $\varpi(t)$ to yield a scaled signal denoted as $\mathcal{F}(t) = K(\varpi).\varpi(t)$. The resultant scaled signal $\mathcal{F}(t)$ is subsequently introduced into the linear FOPID controller, which, in turn, formulates the control signal. It is crucial to emphasize that the nonlinear gain encompasses a wide range of possibilities, encompassing various general nonlinear functions of the input signal. Therefore, there exists a diverse set of options for selecting the appropriate nonlinear gain. The input to the plant, denoted as $u(t)$, can be effectively governed by the following nonlinear control law [40]:

$$ \begin{aligned} & u(t) = \mathcal{F}_1(\varpi(t)) + \mathcal{F}_2(D^{\mu}\varpi(t)) + \mathcal{F}_3(D^{-\lambda}\varpi(t)), \\ & \mathcal{F}_i(\cdot) = \kappa_i(\cdot)|\cdot|^{\beta_i}\mathrm{sign}(\cdot) \\ & \quad \cdot = \varpi(t), D^{\mu}\varpi(t) \quad \text{or} \quad D^{-\lambda}\varpi(t), \quad \text{and} \quad i = 1,2,3, \\ & \kappa_i(\cdot) = K_{i1} + \frac{K_{i2}}{1 + e^{(\cdot)^2 \alpha_i}}. \end{aligned} \quad (23) $$

The proposed formulation of the FOPID controller introduces nonlinear gain components denoted by positive constants K_{i1}, K_{i2}, α_i and β_i. These parameters serve a crucial function in enhancing the responsiveness of the controller toward minor discrepancies. As the error decreases toward zero, the nonlinear gain component stabilizes at the upper boundary determined by the expression $K_{i1} + K_{i2}/2$. Conversely, when encountering significant errors, the nonlinear gain tends toward the lower threshold as indicated by K_{i1}. It is crucial to emphasize that the nonlinear gain element is restricted to the range of $[K_{i1}\ K_{i1} + K_{i2}/2]$, ensuring compliance with the predetermined range. The design of the nonlinear FOPID controller in this paper aligns with the methodology delineated in a prior study on nonlinear PID controllers [40].

3.1. *IT2-FLCs structure*

The controller system comprises key components such as the fuzzifier, rule base, inference engine, type reducer and defuzzifier, each serving specific functions as illustrated in Fig. 4. The fuzzifier transforms crisp inputs into linguistic variables, facilitating their processing within the fuzzy system. Subsequently, the inference engine uses the output of the IT2-FLC system to amplify control actions based on expert-encoded rules, enabling intelligent decision-making and optimizing system performance. Additionally, input and output scaling factors allow for fine-tuning the impact of variables on the control signals and the controlled system, thereby enhancing the overall functionality of the IT2-FLC system.

A generalized rule of an IT2-FLS, comprising N rules ($i = 1, \ldots, N$), is formulated as stated by [19]:

$$ R^i : \text{IF } \upsilon_1 \text{ is } \tilde{A}_2^i \quad \text{and} \quad \upsilon_2 \text{ is } \tilde{A}_2^i, \text{THEN } \varpi^i = Y^i, \quad (24) $$

where υ_1 and υ_2 denote the input variables, ϖ signifies the output variable, Y^i denotes the parameters of the

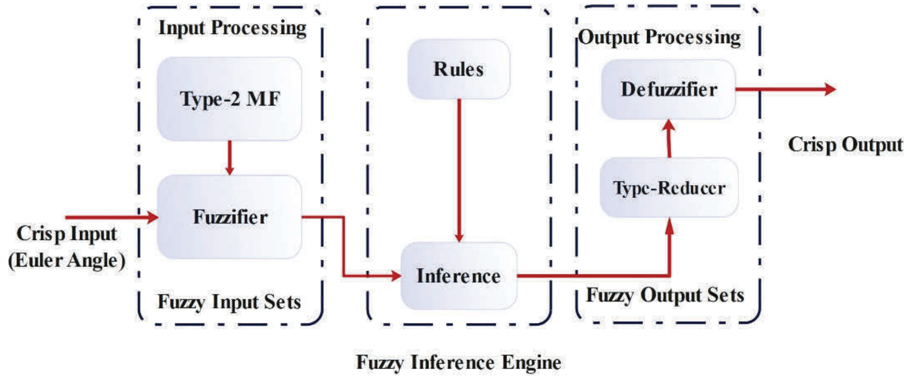

Fig. 4. Structure of IT2-FLCs.

consequent part of the fuzzy system, and $\tilde{A}_1^i, \tilde{A}_2^j$ indicate the type-2 fuzzy sets for the first and second inputs correspondingly. The associated fuzzy MFs for $\tilde{A}_1^i$, and $\tilde{A}_2^j$ are symbolized as $\tilde{\mu}_1^i$, and μ_2^i, respectively. The type-2 Gaussian MFs are employed in this paper, and they are characterized by their upper and lower MFs as

$$\bar{\mu}_{\tilde{A}_j^i}^{j}(\chi_j) = \exp\left(-\frac{1}{2}\left(\frac{\chi_j - \bar{c}_j^i}{\bar{\sigma}_j^i}\right)^2\right) \chi_j = \upsilon_1 \quad \text{or} \quad \upsilon_2, \tag{25}$$

$$\underline{\mu}_{\tilde{A}_j^i}^{j}(\chi_j) = \exp\left(-\frac{1}{2}\left(\frac{\chi_j - \underline{c}_j^i}{\underline{\sigma}_j^i}\right)^2\right). \tag{26}$$

The values acquired from the upper and lower MFs for the jth input and ith rule are denoted as $\bar{\mu}_{\tilde{A}_j^i}(\chi_j)$ and $\underline{\mu}_{\tilde{A}_j^i}^{j}(\chi_j)$, respectively. A type-2 fuzzy set represents the region bounded by an upper and a lower MF. The centers of Gaussian functions, $\underline{c}_j^i$ and $\bar{c}_j^i$, correspond to the mean values of the lower and upper MFs, respectively. Similarly, $\underline{\sigma}_j^i$ and $\bar{\sigma}_j^i$ refer to the widths of the lower and upper Gaussian functions. The consequent part of rules, Y^i, is expressed as a numerical interval $Y^i = [\underline{Y}^i, \overline{Y}^i]$, where $\underline{Y}^i$ and $\overline{Y}^i$ indicate the lower and upper bounds of the interval. When utilizing the t-norm for inference and employing type reduction for the center-of-set, the antecedents of the ith fuzzy rule can be represented as a numerical interval $\Upsilon^i(\boldsymbol{\chi}) = [\Upsilon_l^i(\boldsymbol{\chi}), \Upsilon_u^i(\boldsymbol{\chi})]$, where $\Upsilon_l^i(\boldsymbol{\chi})$ and $\Upsilon_u^i(\boldsymbol{\chi})$ are specified as follows [36]:

$$\begin{aligned} \Upsilon_u^i(\boldsymbol{\chi}) &= \prod_{j=1}^{2} \bar{\mu}_{\tilde{A}_j^i}^{j}(\chi_j) = \bar{\mu}_{\tilde{A}_1^i}^{1}(\chi_1) * \bar{\mu}_{\tilde{A}_2^i}^{2}(\chi_2) \\ \Upsilon_l^i(\boldsymbol{\chi}) &= \prod_{j=1}^{2} \underline{\mu}_{\tilde{A}_j^i}^{j}(\chi_j) = \underline{\mu}_{\tilde{A}_1^i}^{1}(\chi_1) * \underline{\mu}_{\tilde{A}_2{}^i}^{2}(\chi_2), \end{aligned} \tag{27}$$

where $*$ denotes the algebraic product $(*)$ operator.

The overall output of the fuzzy system may be denoted as the average of its lower and upper limits, based on the Karnik–Mendel (KM) algorithm expressed as follows [41]:

$$\varpi = \frac{\underline{\varpi} + \overline{\varpi}}{2}. \tag{28}$$

Here, $\overline{\varpi}$ and $\underline{\varpi}$ are computed as follows [36]:

$$\begin{aligned} \underline{\varpi} &= \frac{\sum_{i=1}^{L} \Upsilon_u^i \underline{Y}^i + \sum_{i=L+1}^{N} \Upsilon_l^i \underline{Y}^i}{\sum_{i=1}^{L} \Upsilon_u^i + \sum_{i=L+1}^{N} \Upsilon_l^i}, \\ \overline{\varpi} &= \frac{\sum_{i=1}^{R} \Upsilon_l^i \overline{Y}^i + \sum_{i=R+1}^{N} \Upsilon_l^i \overline{Y}^i}{\sum_{i=1}^{R} \Upsilon_l^i + \sum_{i=R+1}^{N} \Upsilon_u^i}, \end{aligned} \tag{29}$$

where L and R denote the switching points, which are identified through the implementation of KM algorithms [41].

This study utilizes a fuzzy system with Gaussian membership functions, employing seven sets for inputs and outputs within a range of -1 to 1. The IT2-FLC features seven distinct membership functions for input variables (NL, NM, NS, Z, PS, PM, PL) as shown in Fig. 5. A rule base of 49 rules is established through trial-and-error, ensuring a smooth system output, as presented in Table 1. The Mamdani min–max method serves as the inference engine, and the centroid method is employed for defuzzification.

The variables K_P and K_D are the scaling factors of the tracking error $(e.)$ and its derivative $(\dot{e})$, respectively. Additionally, variables K_1, K_2 and K_3 are proportional, integral and derivative gains, respectively. Furthermore, the coefficients μ and λ represent the derivative and integration FO, respectively.

3.2. *Grey Wolf Optimizer algorithm*

The Grey Wolf Optimizer (GWO) algorithm is a metaheuristic optimization algorithm inspired by the social hierarchy and hunting mechanisms of grey wolves. The algorithm employs three main types of wolves: alpha, beta and delta, which respectively represent the best, second-best and

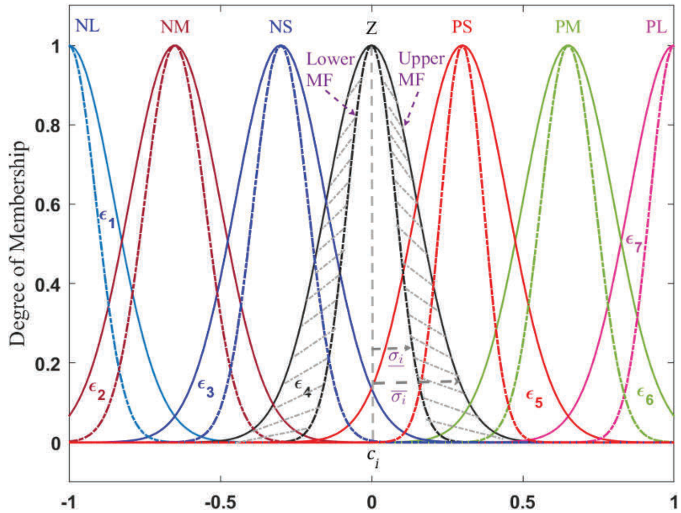

Fig. 5. The used membership functions for the input variables of the interval type-2 fuzzy system.

Table 1. Fuzzy rule base.

	ϖ	υ_1 NL	NM	NS	Z	PS	PM	PL
υ_2	NL	NL	NL	NL	NL	NM	NS	Z
	NM	NL	NL	NL	NM	NS	Z	PS
	NS	NL	NL	NM	NS	Z	PS	PM
	Z	NL	NM	NS	Z	PS	PM	PL
	PS	NM	NS	Z	PS	PM	PL	PL
	PM	NS	Z	PS	PM	PL	PL	PL
	PL	Z	PS	PM	PL	PL	PL	PL

third-best solutions found so far. These wolves undertake exploration and exploitation processes within the search space to iteratively enhance the quality of solutions [42].

During hunting, grey wolves encircle their prey and persistently pursue it until it ceases its movement. The behavioral dynamics are mathematically represented by the following equations:

$$\mathbf{X}(t+1) = \mathbf{X}_P(t) - \mathbf{A} \cdot \mathbf{D}, \tag{30}$$

$$\mathbf{D} = |\mathbf{C} \cdot \mathbf{X}_P(t) - \mathbf{X}(t)|. \tag{31}$$

Here, t denotes the current iteration, $\mathbf{D}$ represents the distance vector, $\mathbf{X}(t)$ is the position vector of a grey wolf and $\mathbf{X}_P(t)$ represents the position vector of the prey. Additionally, $\mathbf{A}$ and $\mathbf{C}$ are coefficient vectors of the grey wolves, defined as

$$\mathbf{A} = 2k \cdot \mathbf{r}_1 - k, \tag{32}$$

$$\mathbf{C} = 2\mathbf{r}_2. \tag{33}$$

Here, the parameter k linearly decreases from 2 to 0 throughout the iterations, while $\mathbf{r}_1$, and $\mathbf{r}_2$ are random vectors within the range [0,1]. The hunting behavior of grey wolves is primarily driven by the alpha wolf, although the beta and delta wolves also contribute to the hunt in certain circumstances. To mathematically simulate this behavior, it is assumed that the alpha, beta and delta wolves possess superior knowledge regarding the potential location of the prey, making them the best candidate solutions.

The top three candidate solutions identified to date are conserved and disseminated among other search agents, including the omegas, in order to adjust their individual positions according to the locations of the most prominent search agents. This updating procedure is delineated by the following expression:

$$\mathbf{X}(t+1) = \frac{\mathbf{X}_1 + \mathbf{X}_2 + \mathbf{X}_3}{3}, \tag{34}$$

where

$$\begin{aligned} &\mathbf{X}_1 = \mathbf{X}_\alpha - \mathbf{A}_1 \cdot \mathbf{D}_\alpha, \quad \mathbf{X}_2 = \mathbf{X}_\beta - \mathbf{A}_2 \cdot \mathbf{D}_\beta, \\ &\mathbf{X}_3 = \mathbf{X}_\delta - \mathbf{A}_3 \cdot \mathbf{D}_\delta. \end{aligned} \tag{35}$$

At a given iteration t, $\mathbf{X}_1, \mathbf{X}_2$ and $\mathbf{X}_3$ represent the first three best solution candidates within the group. $\mathbf{A}_1, \mathbf{A}_2$ and $\mathbf{A}_3$ are defined according to Eq. (31), and $\mathbf{D}_\alpha$, $\mathbf{D}_\beta$ and $\mathbf{D}_\delta$ are position vectors defined as follows:

$$\begin{aligned} &\mathbf{D}_\alpha = |\mathbf{C}_1 \cdot \mathbf{X}_\alpha(t) - \mathbf{X}(t)|, \quad \mathbf{D}_\beta = |\mathbf{C}_2 \cdot \mathbf{X}_\beta(t) - \mathbf{X}(t)|, \\ &\mathbf{D}_\delta = |\mathbf{C}_3 \cdot \mathbf{X}_\delta(t) - \mathbf{X}(t)|. \end{aligned} \tag{36}$$

Here, $\mathbf{X}_\alpha, \mathbf{X}_\beta$ and $\mathbf{X}_\delta$ represent the current positions of the alpha, beta and delta wolves, respectively. $\mathbf{C}_1, \mathbf{C}_2$ and $\mathbf{C}_3$ are coefficient vectors calculated using Eq. (32), representing the alpha, beta and delta wolves, respectively. The parameter k is a control parameter that determines the tradeoff between exploration and exploitation in successive iterations. To update the value of k linearly in each iteration, a proposed approach [43] is to vary k within the range from 2 to 0.

$$k = 2\left(1 - \left(\frac{t}{T}\right)^2\right). \tag{37}$$

In the optimization process, the total number of iterations allowed is denoted by T. Throughout the exploration phase, grey wolves tend to diverge from each other, while during the exploitation phase, they converge toward the best candidate solution. The parameter k plays a crucial role in determining the algorithm's speed and its ability to progress toward the optimal solution. By appropriately selecting the value of k, the algorithm can be expedited in its convergence toward the best candidate solution.

The parameters of the GWO algorithm specific to the considered system are fine-tuned by minimizing the cost functions, as defined in Eq. (38).

$$J(\Xi) = \int |e_\theta(\Xi)|dt + \int |e_\phi(\Xi)|dt + \int |e_\psi(\Xi)|dt. \tag{38}$$

Ξ is the design vector that can be defined for the proposed IT2-FLC as follows:

$$\Xi = [K_P, K_D, K_1, K_2, K_3, \mu, \lambda, \varepsilon_1, \varepsilon_2, \varepsilon_3, \varepsilon_4, \varepsilon_5, \varepsilon_6, \varepsilon_7]^T. \tag{39}$$

The tuning parameters for the proposed IT2-FLC are the input and output scaling factors, and the integral and derivative order as shown in Fig. 2, and antecedent membership function parameters, as shown in Fig. 4.

4. Simulation Results and Discussion

This section provides a thorough assessment of the performance of the designed controller in achieving angular stabilization and precise pulse function tracking during roll and pitch maneuvers. The controller, which combines adaptive IT2-FLC with a nonlinear FOPID controller, is compared with three other controllers: IT2-FLC with FOPID, IT2-FLC with nonlinear FOPID and adaptive IT2-FLC with FOPID. The tracking performance of these controllers is evaluated and compared using three indicators: Maximum Absolute Error (MAE), Integral of the Absolute Error (IAE) and Root Mean Square Error (RMSE) defined in Eqs. (40)–(42), respectively.

$$\mathrm{MAE}(e_.) = \max(|e_.|), \tag{40}$$

$$\mathrm{IAE}(e_.) = \int_0^t |e_.|d\tau, \tag{41}$$

$$\mathrm{RMSE}(e_.) = \sqrt{\frac{\int_0^t |e_.|^2 d\tau}{t}}. \tag{42}$$

In this study, a 3 Degree-of-Freedom (DoF) quadrotor stand is utilized to conduct Hardware-in-the-Loop (HIL) experiments, as depicted in Fig. 6. The quadrotor platform has an angular range of ± 35 degrees along both the roll and pitch axes, enabling unrestricted rotation on the yaw axis. To measure these angles, a combination of an MPU6050 module and an Arduino Uno microcontroller is employed. The Arduino Uno utilizes the serial communication protocol to establish a communication interface with the computer. This interface operates at a speedy baud rate of 115,200 bits per second (bps). The Arduino Uno transmits angular feedback data to the computer and receives corresponding control inputs, which are used to generate velocity commands for the propulsion mechanism. The propulsion setup comprises Emax RS2306 brushless motors, 30 Amps electronic speed controllers, and 5-inch propellers. The control inputs are derived from a predefined control algorithm implemented within the MATLAB/Simulink environment. The HIL control system operates with a sampling frequency of 50 Hz. The main goal of this study is to examine the effectiveness of the controller in achieving angular stabilization and accurately tracking reference commands during roll and pitch maneuvers. The dynamic model of the quadrotor is presented in Table 2.

To optimize the gain parameters, the GWO algorithm is utilized, aiming to minimize the objective function defined in Eq. (38). To accomplish this objective, the tunable gain parameters of the proposed controllers need to be fine-tuned, and the membership functions must be optimized.

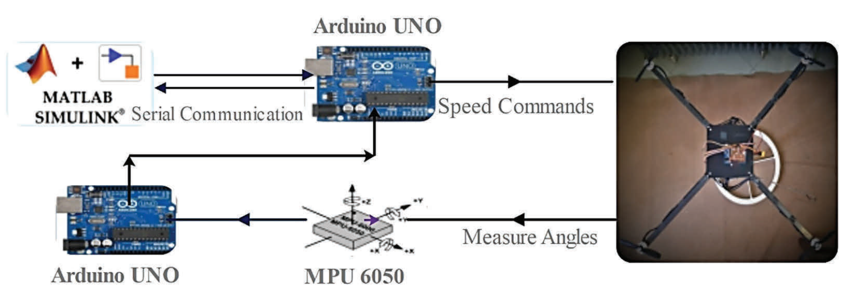

Fig. 6. The hardware in the loop diagram.

Table 2. Quadrotor dynamic model parameters.

Symbol	Name	Value	Unit
$\boldsymbol{I_{xx}}$	Quadrotor moment of inertia around the x-axis	0.007	Kgm^2
$\boldsymbol{I_{yy}}$	Quadrotor moment of inertia around the y-axis	0.007	Kgm^2
$\boldsymbol{I_{zz}}$	Quadrotor moment of inertia around the z-axis	0.012	Kgm^2
$\boldsymbol{L}$	Quadrotor arm length	0.17	m
$\boldsymbol{m}$	Quadrotor mass	0.68	Kg
$\boldsymbol{b}$	Thrust constant	1.34×10^{-5}	Ns^2
$\boldsymbol{d}$	Drag constant	5.8×10^{-7}	Nms^2
$\boldsymbol{J_r}$	Rotor moment of inertia	5.6×10^{-5}	Kgm^2
$\boldsymbol{K_{tm}}$	Motor torque constant	0.025	Nm/A
$\boldsymbol{K_{em}}$	Motor electrical constant	0.025	Vs/Rad
$\boldsymbol{R_m}$	Motor winding resistance	0.1	Ω

Table 3. The uncertainty bounds of the Gaussian MF parameters.

MF parameters for v_1 and v_2	NF	NM	NS	Z	PS	PM	PL
$\underline{\mathbf{c}}$	—	−0.95	−0.5	−0.1	0.1	0.5	—
$\overline{\mathbf{c}}$	—	−0.5	−0.1	0.1	0.5	0.95	—
$\underline{\boldsymbol{\sigma}}$	0.1	0.1	0.1	0.1	0.1	0.1	0.1
$\overline{\boldsymbol{\sigma}}$	0.2	0.2	0.2	0.2	0.2	0.2	0.2

The GWO algorithm is used offline for optimizing control parameters. During the execution of the GWO algorithm, the following parameters are selected: 30 search agents, a maximum of 100 iterations, and 30 runs, as suggested in the original GWO algorithm. The ranges of uncertainty for the Gaussian MF parameters, comprising the center (c) and the width (σ) of a fuzzy set, are delineated in Table 3.

Table 4 presents a detailed of the optimized controller gains and membership function parameters specifically designed for the attitude control of the quadrotor. These optimized parameters are specifically tailored to be utilized in the proposed controllers, which are aimed at achieving precise control over the quadrotor's orientation.

To achieve optimal control performance, the controller parameters are determined offline using optimization techniques. In this study, the GWO algorithm is utilized to optimize the controller parameters. Simulations are conducted to evaluate the controller's performance by tracking a pulse function applied to the roll and pitch angles during a quadrotor maneuver. The tracking results are presented in Fig. 7.

Table 4. Optimal controller gains and MF parameters for attitude scenario.

Controller	Fine-tuned gain parameters of the controllers, and the MFs parameters							
IT2-FLC+FOPID		K_p	K_D	K_1	K_2	K_3	μ	λ
	Roll	1.7	2.1	3.4	0.51	1.3	1.2	0.8
	Pitch	5.8	2.9	8.1	1.12	1.9	1.1	0.9
	Yaw	1.8	2.4	12.7	0.08	0.7	1.9	0.7
		c_{NL}	c_{NM}	c_{NS}	c_Z	c_{PS}	c_{PM}	c_{PL}
	For v_1	0.18	0.16	0.15	0.16	0.16	0.16	0.17
	v_2	0.17	0.16	0.15	0.16	0.15	0.17	0.16
		σ_{NL}	σ_{NM}	σ_{NS}	σ_Z	σ_{PS}	σ_{PM}	σ_{PL}
	For v_1	−1	−0.61	−0.31	0	0.31	0.62	1
	v_2	−1	−0.64	−0.35	0	0.34	0.63	1

Table 4. (*Continued*)

Controller	Fine-tuned gain parameters of the controllers, and the MFs parameters											
IT2-FLC+Nonlinear FOPID		K_p	K_D	K_{11}	K_{12}	α_1	β_1	K_{21}	K_{22}	α_2	β_2	
	Roll	1.5	1.8	2.9	0.04	2.7	5.8	0.4	0.01	0.1	0.2	
	Pitch	5.6	2.6	7.6	0.21	3.4	5.6	1.1	0.02	0.3	0.4	
	Yaw	1.9	2.5	10.9	1.5	4.9	5.9	0.06	0.01	0.1	0.1	
		K_{31}	K_{32}	α_3	β_3	μ	λ					
	Roll	1.4	0.03	0.8	1.2	1.1	0.9					
	Pitch	1.7	0.06	1.1	1.3	1.3	0.9					
	Yaw	0.6	0.02	0.2	0.9	1.8	0.6					
		c_{NL}	c_{NM}	c_{NS}	c_Z	c_{PS}	c_{PM}	c_{PL}				
	For v_1	0.17	0.15	0.15	0.16	0.16	0.15	0.17				
	v_2	0.17	0.16	0.16	0.17	0.15	0.17	0.17				
		σ_{NL}	σ_{NM}	σ_{NS}	σ_Z	σ_{PS}	σ_{PM}	σ_{PL}				
	For v_1	−1	−0.60	−0.31	0	0.31	0.59	1				
	v_2	−1	−0.62	−0.33	0	0.32	0.61	1				
Adaptive IT2-FLC+FOPID		γ_{Pi}	γ_{Di}	λ_i	K_1	K_2	K_3	μ	λ			
	Roll	17.2	0.1	8	4.3	0.48	1.1	1.0	0.9			
	Pitch	25.1	0.7	6	6.8	1.01	1.6	1.3	0.7			
	Yaw	13.8	6	4	11.4	0.09	0.8	1.6	0.5			
		c_{NL}	c_{NM}	c_{NS}	c_Z	c_{PS}	c_{PM}	c_{PL}				
	For v_1	0.17	0.16	0.15	0.16	0.16	0.15	0.17				
	v_2	0.18	0.16	0.15	0.16	0.15	0.16	0.18				
		σ_{NL}	σ_{NM}	σ_{NS}	σ_Z	σ_{PS}	σ_{PM}	σ_{PL}				
	For v_1	−1	−0.58	−0.31	0	0.30	0.59	1				
	v_2	−1	−0.60	−0.32	0	0.30	0.60	1				
Adaptive IT2-FLC+Nonlinear FOPID		γ_{Pi}	γ_{Di}	λ_i	K_{11}	K_{12}	α_1	β_1	K_{21}	K_{22}	α_2	β_2
	Roll	15.4	0.2	6	2.7	0.03	2.4	5.1	0.3	0.01	0.1	0.1
	Pitch	23.1	0.6	5	7.1	0.24	3.1	4.9	0.9	0.01	0.2	0.2
	Yaw	9.8	5.3	3	11.1	1.2	4.5	5.2	0.04	0.01	0.1	0.1
	Roll	K_{31}	K_{32}	α_3	β_3	μ	λ					
	Pitch	1.2	0.02	0.5	0.9	1.3	0.6					
	Yaw	1.5	0.04	0.8	0.8	1.1	0.8					
		c_{NL}	c_{NM}	c_{NS}	c_Z	c_{PS}	c_{PM}	c_{PL}				
	For v_1	0.15	0.15	0.15	0.16	0.15	0.15	0.15				
	v_2	0.16	0.15	0.15	0.16	0.15	0.16	0.15				
		σ_{NL}	σ_{NM}	σ_{NS}	σ_Z	σ_{PS}	σ_{PM}	σ_{PL}				
	For v_1	−1	−0.58	−0.30	0	0.30	0.58	1				
	v_2	−1	−0.59	−0.31	0	0.30	0.58	1				

The results show that incorporating both adaptive structures and nonlinear gain significantly enhances tracking performance. However, the nonlinear gain alone has a more pronounced effect on improving tracking accuracy compared to the adaptive structure. This underscores the importance of nonlinear gain in managing the quadrotor's dynamic response, enabling robust and precise maneuverability.

The time responses of the sliding surface parameters, as illustrated in Fig. 8, demonstrate that each parameter gradually converges to its respective constant value over time. This convergence indicates that the system successfully achieves a stable state, with the sliding surface parameters stabilizing at fixed values.

This study presents experimental results on the stabilization and precise tracking of pulse functions in the roll and pitch angles during quadrotor maneuvers, as depicted in Fig. 9. Noteworthily, in this specific experimental setting, the quadrotor's yaw orientation angle remains constant. All proposed control strategies have effectively tracked the

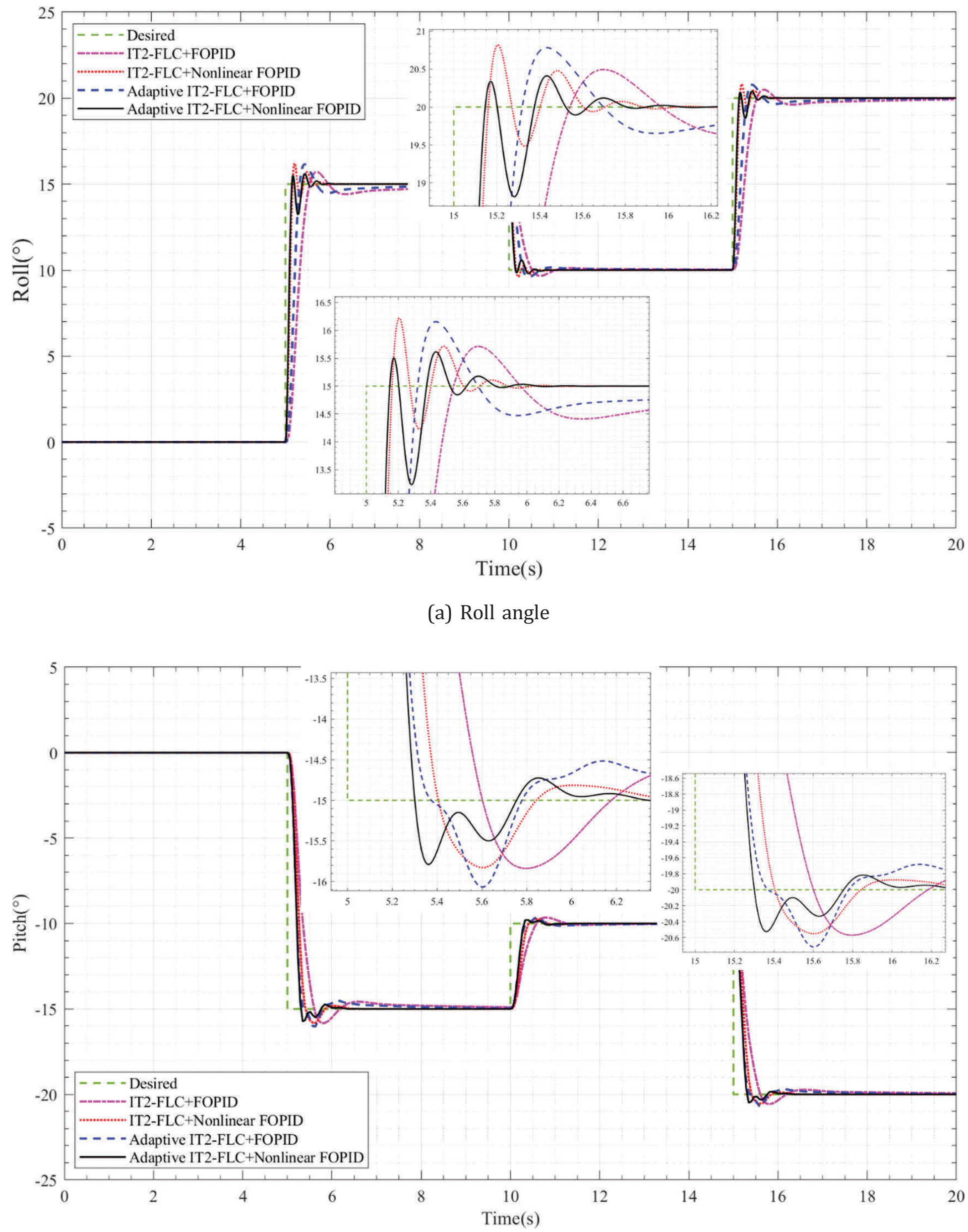

(a) Roll angle

(b) Pitch angle

Fig. 7. Attitude tracking performance of the proposed controllers in the simulation study.

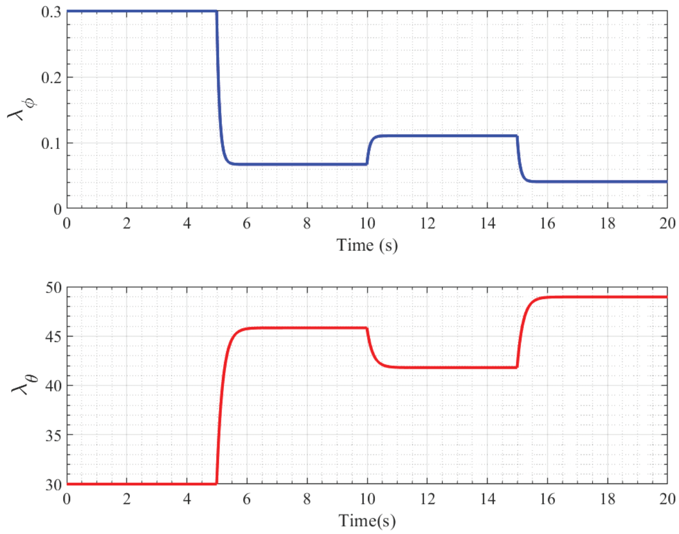

Fig. 8. Variations of sliding surface parameters during the simulation study.

pulse functions during the roll and pitch quadrotor maneuvers in practical scenarios. The findings reveal that the adaptive IT2-FLC combined with the nonlinear FOPID controllers demonstrates superior performance compared to other control methods. The incorporation of nonlinear gain in the FOPID controllers and adaptability in the scaling coefficients of the IT2-FLC positively impact tracking performance. Moreover, the nonlinear gain in the FOPID controllers proves more effective than the adaptive feature of the scaling coefficients associated with the IT2-FLC's input variables. Nevertheless, it is recognized that despite attempts to mitigate external disturbances, like isolating the interface board with anti-vibration foam, mechanical vibrations introduced fluctuations in the controller's practical response. These vibrations influenced the gyroscope sensor, thereby contributing to fluctuations observed in the controller's response.

The time history of the ESC values recorded during the test is illustrated in Fig. 10. Additionally, Fig. 10 showcases the corresponding tracking errors linked to these maneuvers.

Upon examining the attitude tracking error depicted in Fig. 11, one can discern that the adaptive IT2-FLC + nonlinear FOPID controllers demonstrate significant advantages compared to the alternative controllers across all DoF attitude angles. These advantages manifest in diminished overshoot and enhanced response speed, signifying superior performance.

For a thorough evaluation of the controllers' performance, Table 5 is included, showcasing three customized performance metrics — IAE, MAE and RMSE, tailored specifically for the attitude dynamics under consideration. The results obtained from the evaluation reveal that the proposed adaptive IT2-FLC + nonlinear FOPID controllers exhibit substantial improvement in tracking the attitude maneuver in the roll, pitch and yaw angles when compared to the other proposed controllers. This improvement is reflected in the significantly lower values of the IAE, and RMSE indices, indicating enhanced accuracy and precision in tracking the desired attitude maneuvers.

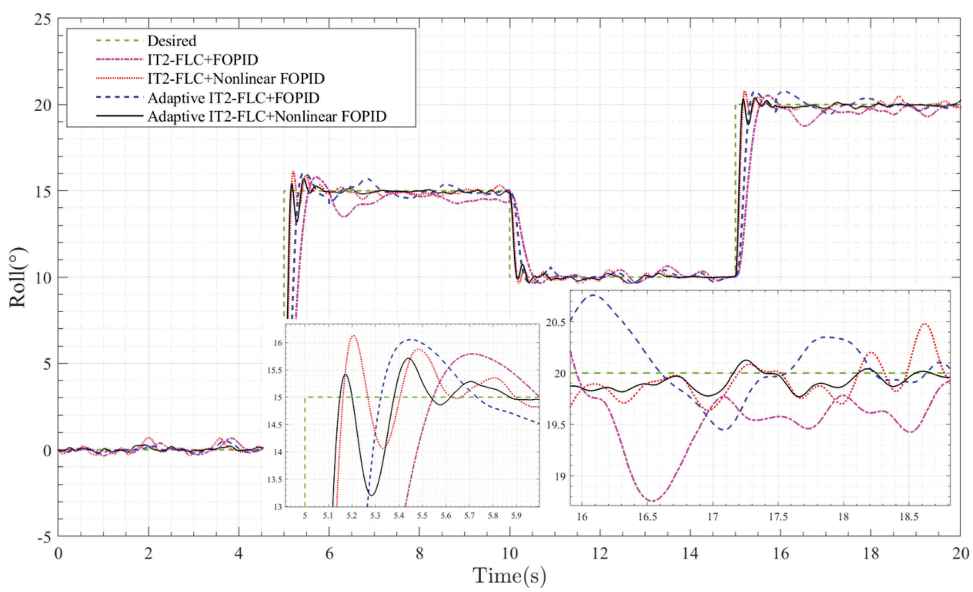

(a) Roll angle

Fig. 9. Attitude tracking of the proposed controllers in HIL test.

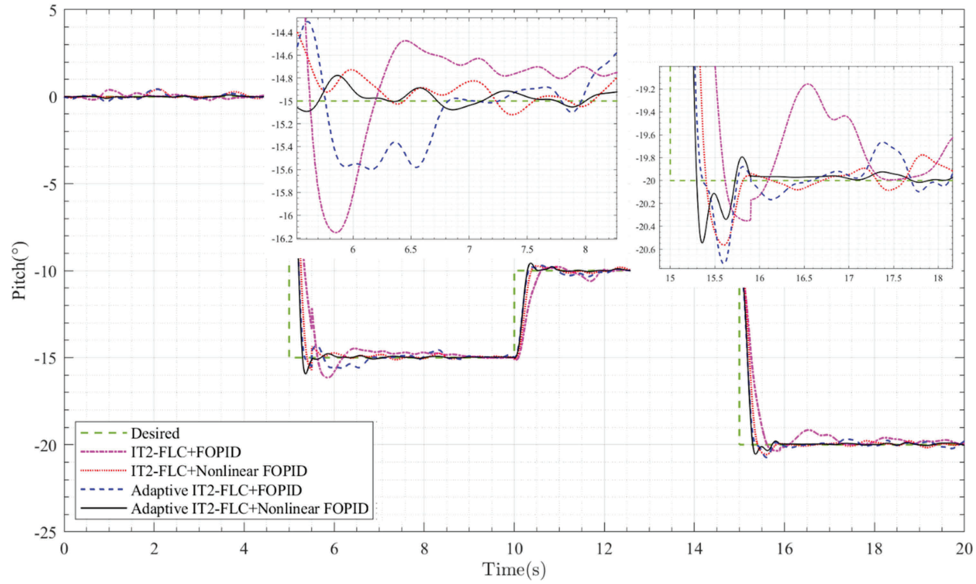

(b) Pitch angle

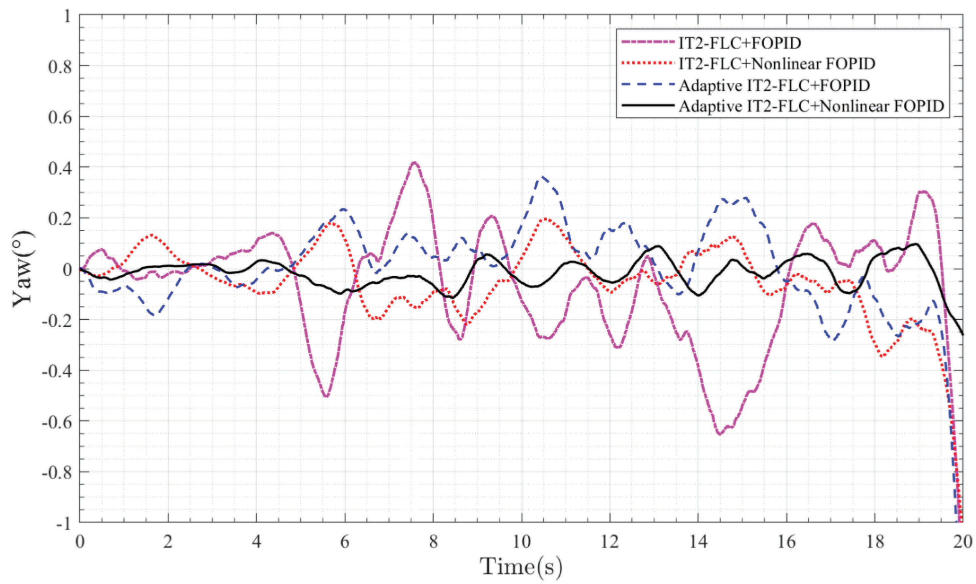

(c) Yaw angle

Fig. 9. (*Continued*)

The performance of the controllers is analyzed by comparing the percentage variation of IAE, MAE and RMSE indices for roll, pitch and yaw axes relative to the baseline controller (IT2-FLC + FOPID). For the roll axis, the IT2-FLC + Nonlinear FOPID achieves a 55.08% reduction in IAE and a 40.80% reduction in RMSE compared to the baseline controller, indicating the significant contribution of nonlinear gain. In contrast, the Adaptive IT2-FLC + FOPID, which incorporates an adaptive structure without nonlinear gain, results in a smaller IAE improvement of 34.62% and RMSE reduction of 17.24%. This shows that nonlinear gain alone has a stronger impact on improving performance in roll axis tracking. However, when both adaptive structure and nonlinear gain are combined in the Adaptive IT2-FLC + Nonlinear FOPID, the IAE and RMSE reductions reach 67.16% and 45.21%, respectively, surpassing the improvements achieved by either approach alone. This synergy suggests that the adaptive structure enhances the

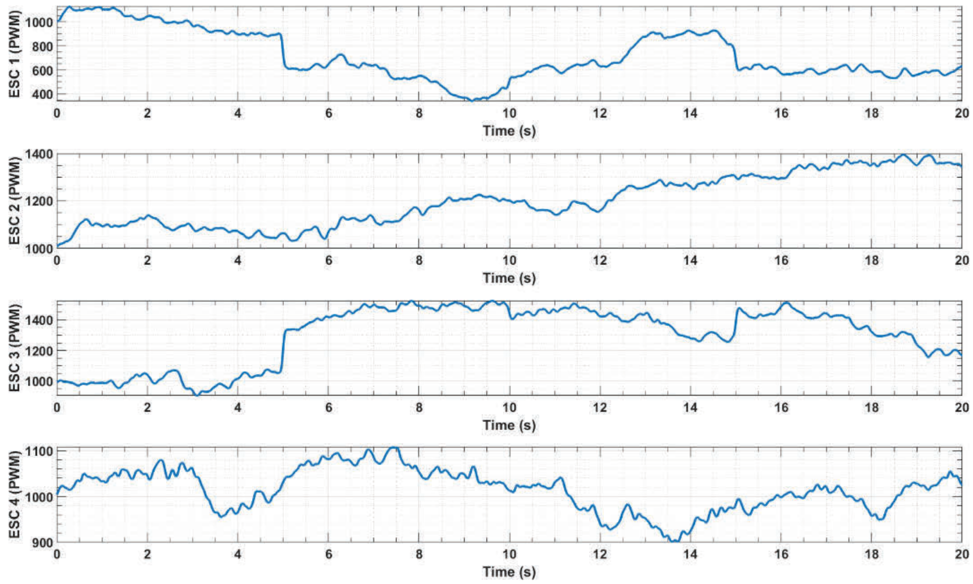

Fig. 10. Time history of electronic speed control for all motors.

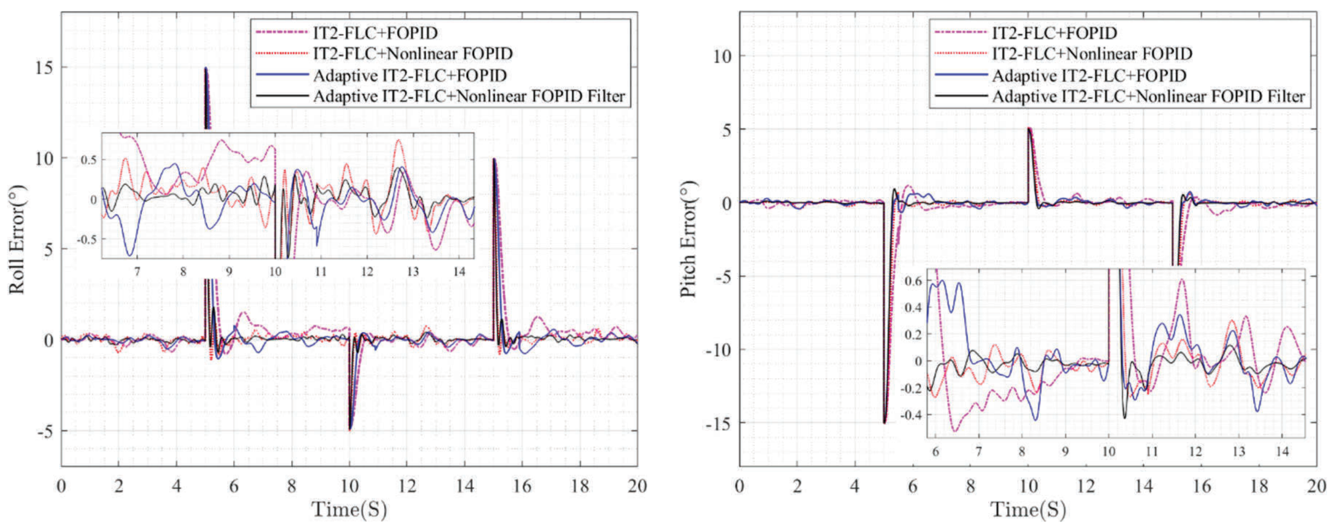

(a) Roll angle error

(b) Pitch angle error

Fig. 11. Attitude tracking errors.

Table 5. Controllers' performance in terms of IAE, MAE and RMSE.

	Roll			Pitch			Yaw		
Controller	IAE	MAE	RMSE	IAE	MAE	RMSE	IAE	MAE	RMSE
IT2-FLC+FOPID	101.38	14.93	5.22	37.60	15.00	3.43	1.69	0.64	0.18
IT2-FLC+Nonlinear FOPID	45.56	14.90	3.09	23.57	15.02	2.81	1.05	0.34	0.11
Adaptive IT2-FLC+FOPID	66.317	14.97	4.32	26.23	15.05	3.14	1.26	0.36	0.14
Adaptive IT2-FLC+Nonlinear FOPID	33.24	14.90	2.86	18.87	15.02	2.76	0.43	0.1	0.04

performance of the nonlinear gain by dynamically adjusting the control parameters to better handle variations in the system dynamics. For the pitch axis, the IT2-FLC+ Nonlinear FOPID reduces IAE by 37.36% and RMSE by 18.10%, demonstrating the effectiveness of nonlinear gain. On the other hand, the Adaptive IT2-FLC+FOPID achieves a smaller IAE reduction of 30.27% and a modest RMSE improvement of 8.45%. This again highlights that nonlinear gain has a more pronounced effect on pitch tracking performance compared to the adaptive structure alone. However, when the adaptive structure is combined with nonlinear gain in the Adaptive IT2-FLC+Nonlinear FOPID, the IAE and RMSE reductions reach 49.77% and 19.53%, respectively. This indicates that the adaptive structure further optimizes the performance of the nonlinear gain by adjusting the control system to varying conditions, albeit the improvement is less dramatic compared to the roll axis. For the yaw axis, the IT2-FLC+Nonlinear FOPID achieves reductions of 37.87% in IAE, 46.88% in MAE and 38.89% in RMSE, significantly outperforming the adaptive structure alone. The Adaptive IT2-FLC + FOPID delivers smaller improvements of 25.44% in IAE, 43.75% in MAE and 22.22% in RMSE. However, the combination of adaptive structure and nonlinear gain in the Adaptive IT2-FLC+ Nonlinear FOPID leads to dramatic improvements of 74.56% in IAE, 93.75% in MAE and 77.78% in RMSE. This highlights the dominant role of nonlinear gain in enhancing yaw tracking performance while showing that the adaptive structure complements it by further fine-tuning the control system to reduce errors under varying dynamic conditions. Across all axes, nonlinear gain alone consistently achieves substantial improvements in IAE and RMSE, demonstrating its significant impact on tracking precision. In contrast, the adaptive structure alone has a more modest effect on performance, with relatively smaller improvements in the indices. However, when the adaptive structure and nonlinear gain are combined, the performance consistently surpasses that of either approach alone. This indicates a synergistic effect, where the adaptive structure enhances the ability of nonlinear gain to dynamically respond to changes in system dynamics and disturbances. Thus, while nonlinear gain is the dominant factor in improving tracking performance, the addition of an adaptive structure provides complementary benefits.

5. Conclusion

This study presented the design and implementation of a novel controller, namely the adaptive IT2-FLC, integrated with a nonlinear FOPID controller, for the attitude control of a quadrotor robot. The scaling coefficients of the fuzzy system were adapted using a sliding surfaces-based adaptive mechanism, enabling real-time adjustment of controller parameters. The fuzzy system was also integrated with a nonlinear FOPID, allowing for dynamic adjustment of its parameters to enhance responsiveness and stability. The GWO algorithm was employed to determine the optimal controller parameters and fuzzy system's membership function parameters. Subsequently, experimental tests using a 3 DoF quadrotor stand were conducted through HIL simulation to assess the efficacy of the proposed controllers. The results demonstrated that the adaptive IT2-FLC+nonlinear FOPID controllers outperformed the other proposed controllers, as indicated by lower IAE, MAE and RMSE indices, showcasing enhanced accuracy and precision in tracking attitude maneuvers. Furthermore, the incorporation of the nonlinear gain in the FOPID controllers and the adaptability of the scaling coefficients in the IT2-FLC positively impacted the tracking performance. Furthermore, it was observed that the nonlinear gain in the FOPID controllers demonstrated greater effectiveness when compared to the adaptive variation in the scaling coefficients linked to the input variables of the IT2-FLC. The integration of a disturbance observer within a composite control strategy is proposed to further enhance performance in future studies. Considering that MPC is effective in managing uncertainty [44], a promising future direction involves integrating model predictive control with a disturbance observer for disturbance rejection.

Declarations

Funding statement: This research received no specific grant from any funding agency in the public, commercial, or not-for-profit sectors

Conflict of Interests The authors declare that there is no competing financial interest or personal relationship that could have appeared to influence the work reported in this paper.

Data availability statement: All necessary mathematical formulae and parameter values needed to replicate the results are given in the text.

Ethics approval: Not applicable.

Consent to participate: Not applicable.

Consent for publication: Not applicable.

References

[1] H. Jeon, J. Song, H. Lee and Y. Eun, Modeling quadrotor dynamics in a wind field, *IEEE/ASME Trans. Mechatron.* **26**(3) (2020) 1401–1411.

[2] S. Zeghlache, H. Rahali, A. Djerioui, L. Benyettou and M. F. Benkhoris, Robust adaptive backstepping neural networks fault tolerant control for mobile manipulator UAV with multiple uncertainties, *Math. Comput. Simul.* **218** (2024) 556–585.

[3] K. Guo, W. Zhang, Y. Zhu, J. Jia, X. Yu and Y. Zhang, Safety control for quadrotor UAV against ground effect and blade damage, *IEEE Trans. Ind. Electron.* **69**(12) (2022) 13373–13383.

[4] C. D. McKinnon and A. P. Schoellig, Estimating and reacting to forces and torques resulting from common aerodynamic disturbances acting on quadrotors, *Robot. Auton. Syst.* **123** (2020) 103314.

[5] D. Wang, Q. Pan, Y. Shi, J. Hu and C. Zhao, Efficient nonlinear model predictive control for quadrotor trajectory tracking: Algorithms and experiment, *IEEE Trans. Cybern.* **51**(10) (2021) 5057–5068.

[6] G. Cao, E. M. K. Lai and F. Alam, Gaussian process model predictive control of an unmanned quadrotor, *J. Intell. Robot. Syst.* **88** (2017) 147–162.

[7] L. Besnard, Y. B. Shtessel and B. Landrum, Quadrotor vehicle control via sliding mode controller driven by sliding mode disturbance observer, *J. Franklin Inst.* **349**(2) (2012) 658–684.

[8] X. Wu, B. Xiao and Y. Qu, Modeling and sliding mode-based attitude tracking control of a quadrotor UAV with time-varying mass, *ISA Trans.* **124** (2022) 436–443.

[9] Ghasemi and M. M. Azimi, Adaptive fuzzy PID control based on nonlinear disturbance observer for quadrotor, *J. Vib. Control* **29**(13–14) (2023) 2965–2977.

[10] M. J. Mahmoodabadi and N. R. Babak, Robust fuzzy linear quadratic regulator control optimized by multi-objective high exploration particle swarm optimization for a 4 degree-of-freedom quadrotor, *Aerosp. Sci. Technol.* **97** (2020) 105598.

[11] L. Zhou, J. Zhang, J. Dou and B. Wen, A fuzzy adaptive backstepping control based on mass observer for trajectory tracking of a quadrotor UAV, *Int. J. Adapt. Control Signal Process.* **32**(12) (2018) 1675–1693.

[12] Ghasemi, F. Parivash and S. Ebrahimian, Autonomous landing of a quadrotor on a moving platform using vision-based FOFPID control, *Robotica* **40**(5) (2022) 1431–1449.

[13] V. P. Tran, F. Santoso, M. A. Garratt and I. R. Petersen, Adaptive second-order strictly negative imaginary controllers based on the interval type-2 fuzzy self-tuning systems for a hovering quadrotor with uncertainties, *IEEE/ASME Trans. Mechatron.* **25**(1) (2020) 11–20.

[14] İ. Şahin and C. Ulu, Altitude control of a quadcopter using interval type-2 fuzzy controller with dynamic footprint of uncertainty, *ISA Trans.* **134** (2023) 86–94.

[15] Amirkhani, M. Shirzadeh and T. Kumbasar, Interval type-2 fuzzy cognitive map-based flight control system for quadcopters, *Int. J. Fuzzy Syst.* **22** (2020) 2504–2520.

[16] W. Xian, Q. Qi, W. Liu, Y. Liu, D. Li and Y. Wang, Control of quadrotor robot via optimized nonlinear type-2 fuzzy fractional PID with fractional filter: Theory and experiment, *Aerosp. Sci. Technol.* (2024) 109286.

[17] Hailemichael and A. Karimoddini, Development of a robust interval type-2 TSK fuzzy logic controlled UAV platform, *J. Intell. Robot. Syst.* **107**(2) (2023) 27.

[18] Al-Mahturi, F. Santoso, M. A. Garratt and S. G. Anavatti, Self-learning in aerial robotics using type-2 fuzzy systems: Case study in hovering quadrotor flight control, *IEEE Access* **9** (2021) 119520–119532.

[19] T. L. Le, N. V. Quynh, N. K. Long and S. K. Hong, Multilayer interval type-2 fuzzy controller design for quadcopter unmanned aerial vehicles using Jaya algorithm, *IEEE Access* **8** (2020) 181246–181257.

[20] J. Dombi and A. Hussain, Data-driven interval type-2 fuzzy inference system based on the interval type-2 distending function, *IEEE Trans. Fuzzy Syst.* **31** (2022) 2345–2359.

[21] M. Shirzadeh, A. Amirkhani, N. Tork and H. Taghavifar, Trajectory tracking of a quadrotor using a robust adaptive type-2 fuzzy neural controller optimized by cuckoo algorithm, *ISA Trans.* **114** (2021) 171–190.

[22] F. Parivash and A. Ghasemi, Trajectory tracking control for a quadrotor using fuzzy PID control scheme, in *Proc. 4th Int. Conf. Knowledge-Based Engineering and Innovation (KBEI)* (IEEE, 2017), pp. 0553–0558.

[23] Li, Y. Wang and X. Yang, Adaptive fuzzy control of a quadrotor using disturbance observer, *Aerosp. Sci. Technol.* **128** (2022) 107784.

[24] M. M. Ferdaus, M. Pratama, S. G. Anavatti, M. A. Garratt and E. Lughofer, PAC: A novel self-adaptive neuro-fuzzy controller for micro aerial vehicles, *Inf. Sci.* **512** (2020) 481–505.

[25] V. Nekoukar and N. M. Dehkordi, Robust path tracking of a quadrotor using adaptive fuzzy terminal sliding mode control, *Control Eng. Pract.* **110** (2021) 104763.

[26] Yu, S. Ma, Y. J. Liu, Z. Wang and C. P. Chen, Finite-time adaptive fuzzy backstepping control for quadrotor UAV with stochastic disturbance, *IEEE Trans. Autom. Sci. Eng.* **21** (2023) 1335–1345.

[27] D. Timis, C. I. Muresan and E. H. Dulf, Design and experimental results of an adaptive fractional-order controller for a quadrotor, *Fract. Fract.* **6**(4) (2022) 204.

[28] M. Labbadi, Y. Boukal and M. Cherkaoui, Path following control of quadrotor UAV with continuous fractional-order super twisting sliding mode, *J. Intell. Robot. Syst.* **100** (2020) 1429–1451.

[29] L. Guettal, A. Chelihi, R. Ajgou and M. M. Touba, Robust tracking control for quadrotor with unknown nonlinear dynamics using adaptive neural network based fractional-order backstepping control, *J. Franklin Inst.* **359**(14) (2022) 7337–7364.

[30] Ansarian and M. J. Mahmoodabadi, Multi-objective optimal design of a fuzzy adaptive robust fractional-order PID controller for a nonlinear unmanned flying system, *Aerosp. Sci. Technol.* **141** (2023) 108541.

[31] H. K. Tran and T. N. Nguyen, Flight motion controller design using genetic algorithm for a quadcopter, *Meas. Control* **51**(3–4) (2018) 59–64.

[32] S. H. Derrouaoui, Y. Bouzid and M. Guiatni, PSO based optimal gain scheduling backstepping flight controller design for a transformable quadrotor, *J. Intell. Robot. Syst.* **102**(3) (2021) 67.

[33] H. Keshavarzpour and A. Ghasemi, Hybrid fuzzy PID sound radiation control of a functionally graded porous GPL-reinforced plate with piezoelectric sensor and actuator layers, *Appl. Math. Model.* (2023).

[34] Z. Cai, J. Lou, J. Zhao, K. Wu, N. Liu and Y. X. Wang, Quadrotor trajectory tracking and obstacle avoidance by chaotic grey wolf optimization-based active disturbance rejection control, *Mech. Syst. Signal Process.* **128** (2019) 636–654.

[35] M. Mjahed and H. Ayad, Quadrotor identification through the cooperative particle swarm optimization-cuckoo search approach, *Comput. Intell. Neurosci.* **2019**(1) (2019) 8925165.

[36] Kaba and E. Kiyak, Artificial bee colony-based Kalman filter hybridization for three-dimensional position estimation of a quadrotor, *Aircr. Eng. Aerosp. Technol.* **92** (2020) 1523–1532.

[37] Z. Lyu, Z. Wang, D. Duan, L. Lin, J. Li, Y. Yang, Y. Chen and Y. Li, Tilting path optimization of tilt quad rotor in conversion process based on ant colony optimization algorithm, *IEEE Access* **8** (2020) 140777–140791.

[38] H. Bhrawy and M. Zaky, Numerical algorithm for the variable-order Caputo fractional functional differential equation, *Nonlinear Dyn.* **85** (2016) 1815–1823.

[39] W. D. Chang and J. J. Yan, Adaptive robust PID controller design based on a sliding mode for uncertain chaotic systems, *Chaos Solitons Fractals* **26**(1) (2005) 167–175.

[40] A. Najm and I. K. Ibraheem, Nonlinear PID controller design for a 6-DOF UAV quadrotor system, *Eng. Sci. Technol. Int. J.* **22** (2019) 1087–1097.

[41] Wu and J. M. Mendel, Enhanced Karnik-Mendel algorithms, *IEEE Trans. Fuzzy Syst.* **17** (2008) 923–934.

[42] S. Mirjalili, S. M. Mirjalili and A. Lewis, Grey wolf optimizer, *Adv. Eng. Softw.* **69** (2014) 46–62.

[43] S. N. Ghorpade, M. Zennaro and B. S. Chaudhari, GWO model for optimal localization of IoT-enabled sensor nodes in smart parking systems, *IEEE Trans. Intell. Transp. Syst.* **22** (2020) 1217–1224.

[44] J. Hu, P. Yan and G. Tan, A two-layer optimal scheduling method for microgrids based on adaptive stochastic model predictive control, *Meas. Sci. Technol.* **36** (2024) 026208, doi: 10.1088/1361-6501/ada39b.